Supplementary Information

Recovering copper from e-waste: recyclable precipitation versus solvent extraction with carbon emission assessment

Susanna S. M. Vance, [1] Efthalia Chatzisymeon,[2] Carole A. Morrison[1]* and Jason B. Love[1]*

[1]EaStCHEM School of Chemistry, University of Edinburgh, Edinburgh EH9 3FJ

[2]School of Engineering, University of Edinburgh, Edinburgh EH9 3FJ

*Carole.Morrison@ed.ac.uk *jason.love@ed.ac.uk

Section 1: Acidic stock solution preparation

Table S1. Preparation of pH 1-5 stock solutions – The details of the single metal stock solutions prepared are given below, indicating the H_2SO_4 concentration of each solution. The pH 3 and pH 4 stock solutions were prepared from the pH 5 solution with dropwise addition of the pH 2 solution to the pH 5 solution. This was done as the volume of H_2SO_4 that would be required to achieve the correct pH (either 3 or 4) was very small and therefore resulted in inaccuracies.

pH	[Cu] / M	[H_2SO_4] / M
1	0.01	0.1
2	0.01	0.01
3	0.01	Prepared from pH 2 and pH 5 soln.
4	0.01	Prepared from pH 2 and pH 5 soln.
5	0.01	0*

* 0.01 M solution of $CuSO_4$ prepared in ultra-pure water

Section 2: Ligand solubility tests

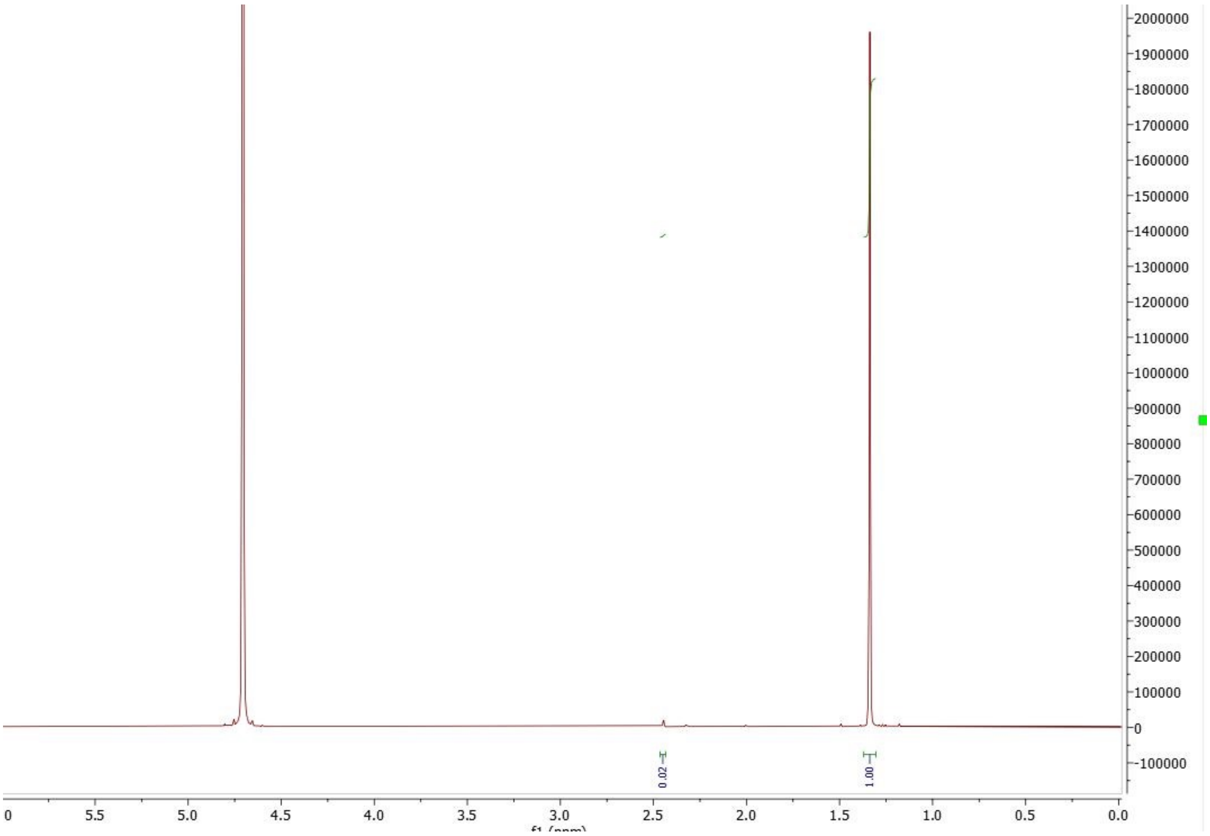

Figure S1: ^{1}H NMR spectrum of L^O in D_2O with tBuOH internal standard. In order to determine the solubility of L^O in aqueous media, an NMR spectrum was recorded in D_2O. A known amount (0.2 mL) of a standard t-BuOH solution (0.05 M in D_2O or H_2O) was added as an internal standard (IS). The following equations were then used to calculate the amount of ligand in each sample, where n_A represents the amount of ligand in the sample in moles and N is the number of nuclei represented by the peaks chosen.

$$n_A = (n_{IS})(r_{A/IS})$$

Where:

$$r_{A/IS} = \frac{(integral_A)/N_A}{(integral_{IS})/N_{IS}}$$

The CH_3 peak was used as the integral for L^O as it was the strongest signal for the ligand (N=6). From this analysis, it was determined that approximately 3% of L^O was dissolved in D_2O.

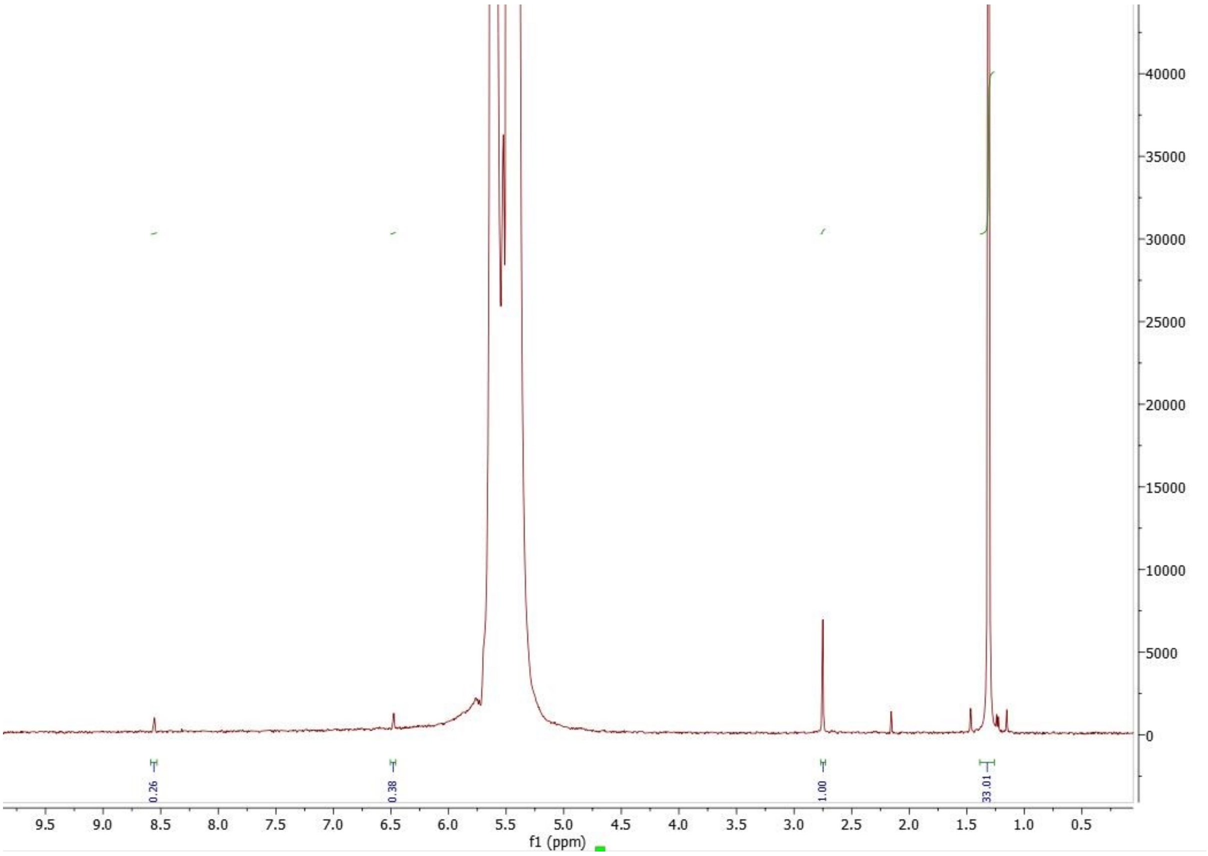

Figure S2: ^{1}H NMR spectrum of L^O in final strip solution with tBuOH internal standard. L^O (0.0224 g, 0.1 mmol) was added to a vial with a solution of $CuSO_4$ (0.02 mmol) and stirred for 1 h. The solution was then centrifuged and the raffinate removed. The precipitate was then washed with DI water (2 mL). The loaded precipitate was then stripped by contacting with a solution of H_2SO_4 (2 M, 2 mL) and stirring for 1 hr. The sample was then centrifuged and the supernatant removed. In order to determine how much ligand remained in this final strip solution, an aliquot (0.5 mL) of this solution was analysed by NMR using tBuOH (0.05 M, 0.2 mL) as an internal standard. The same method as above in Figure S1 was used to determine how much of L^O was dissolved in solution. From this analysis it was determined that 3% of L^O was dissolved in the strip solution. This was calculated using the signal for the CH_3 group (N=6) as this was the most intense signal. It should be noted that the NMR carried out is only semi-quantitative so the solubility data reported is only an estimation. In addition, even after suppression of the solvent peak, a large water signal is still present, which likely skews the integrals reported.

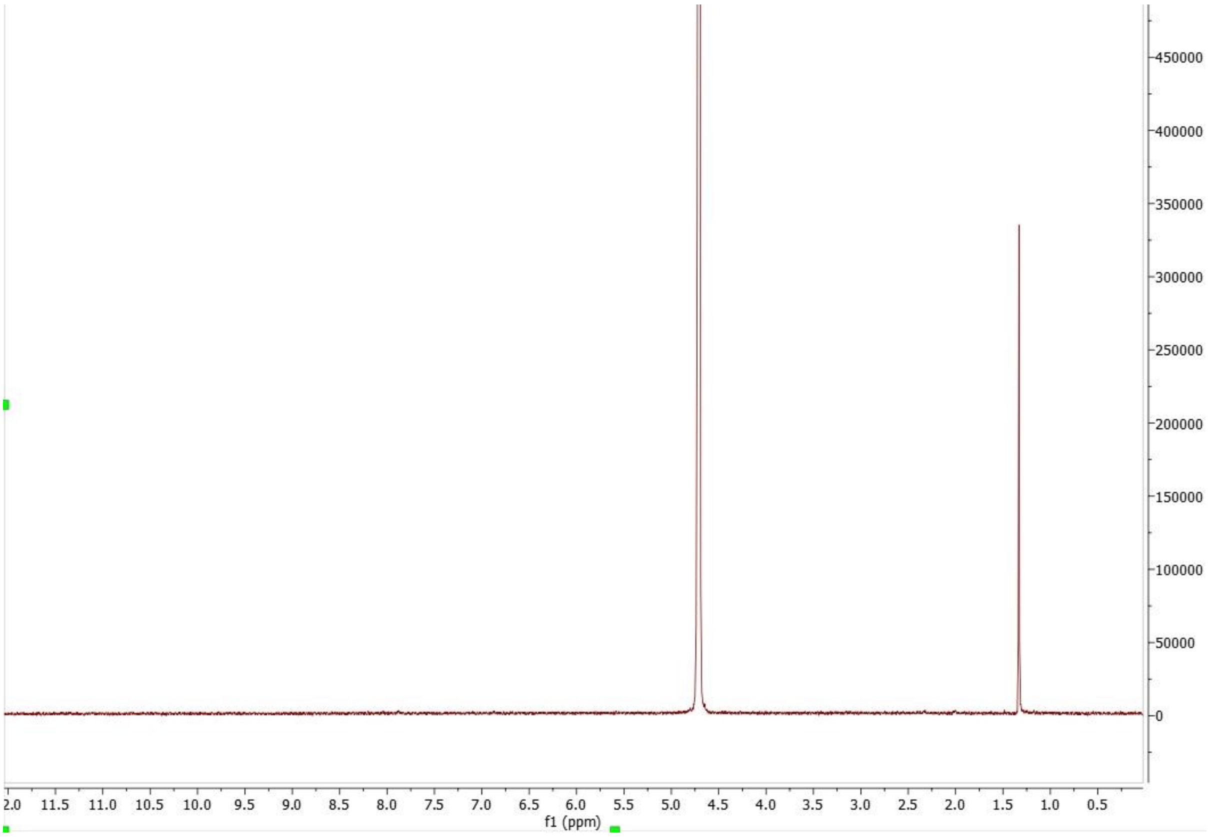

Figure S3: ^{1}H NMR spectrum of L^P in D$_2$O with tBuOH internal standard. The solubility of L^P in aqueous media was also investigated, with an NMR spectrum recorded in D$_2$O. Again tBuOH (2 mL, 0.05 M in D$_2$O) was added as an internal standard (IS). The NMR spectrum showed no evidence of any dissolution of L^P in D$_2$O, with no signals corresponding the ligand protons visible. This suggests that L^P is sparingly soluble in aqueous media and supports the longer timeframe needed for complete precipitation of Cu by this ligand.

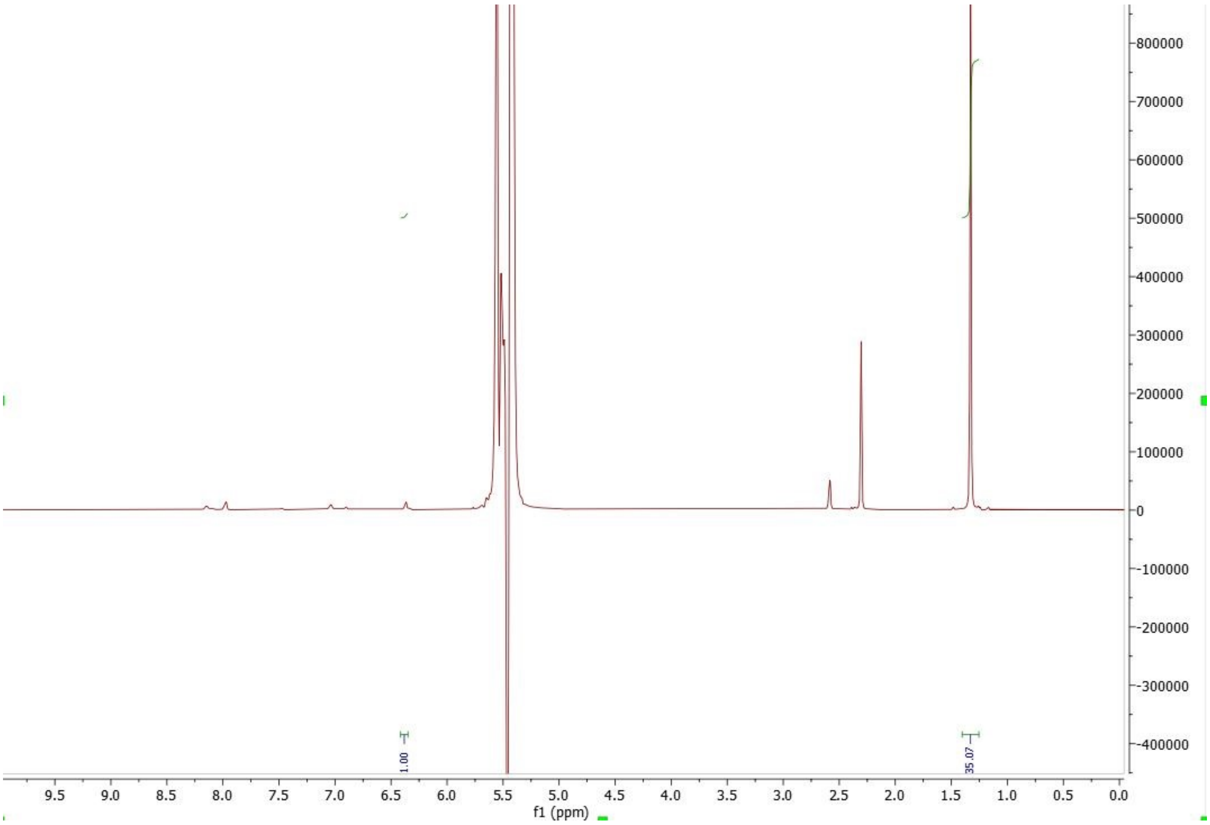

Figure S4: ^{1}H NMR spectrum of L^P in final strip solution with tBuOH internal standard. L^P (0.0242 g, 0.1 mmol) was added to a vial with a solution of $CuSO_4$ (0.02 mmol) and stirred for 1 h. The solution was then centrifuged and the raffinate removed. The precipitate was then washed with DI water (2 mL). The loaded precipitate was then stripped by contacting with a solution of H_2SO_4 (2 M, 2 mL) and stirring for 1 hr. The sample was then centrifuged and the supernatant removed. In order to determine how much ligand remained in this final strip solution, an aliquot (0.5 mL) of this solution was analysed by NMR using tBuOH (0.05 M, 0.2 mL) as an internal standard. The same method as above in Figure S1 was used to determine how much of L^P was dissolved in solution. From this analysis it was determined that 5% of L^P was dissolved in the strip solution. This was calculated using the signal for one of the pyrazole CH groups (N=2). Given all the signals in the spectrum of L^P correspond to either 1H or 2H, this results in a much larger error in the final solubility reported as the signal to noise is much higher, with the signals for all of the L^P protons very small compared to the large residual water peak. As before, the NMR carried out is only semi-quantitative so the solubility data reported is only an estimation. Given the solubility of L^P was lower in aqueous media compared to L^O, which was consistent between both samples, it can be assumed that the solubility reported for L^P in the final strip solution of 5% is a slight overestimation.

Section 3: Extended precipitation experiments

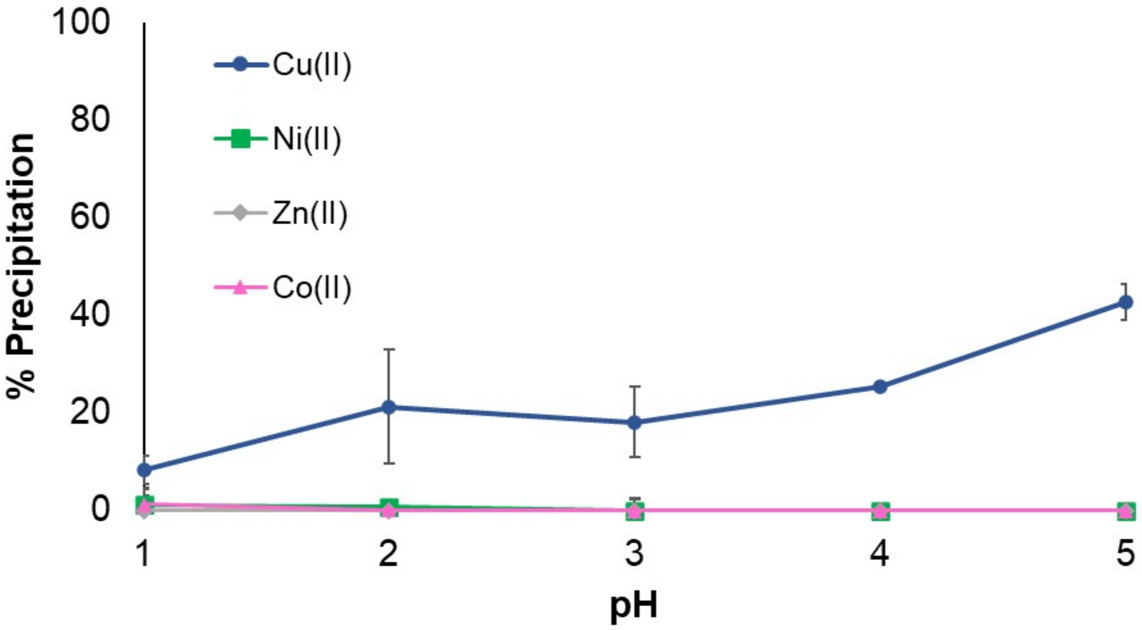

Figure S5. Precipitation plot (%) of [Cu(L^P)]$_n$ from mixed metal solutions over the pH range 1-5 – The precipitation plot above shows the percentage precipitation of copper from mixed-metal solutions over the pH range 1-5 with a 1 h contact with L^P. For complete precipitation of copper by L^P, the contact time must be extended to 24 h.

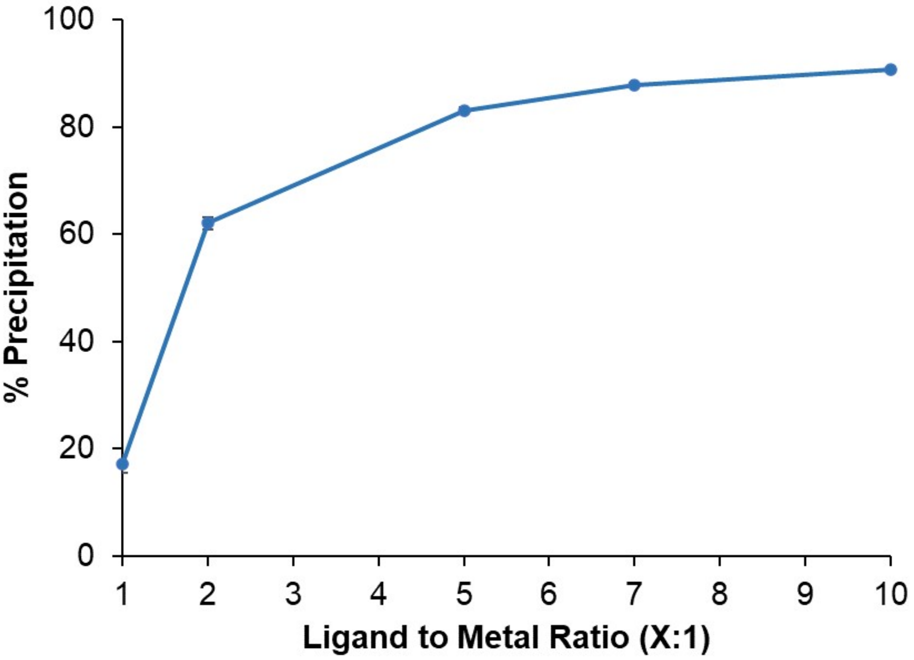

Figure S6. Varying the ligand to copper ratio with L^O– The precipitation plot above shows the percentage precipitation for the ligand:metal screen from 1:1 to 10:1 with L^O. The optimum ratio was 5:1, given near quantitative precipitation was achieved at this ratio whilst minimising the use of a very large excess of ligand.

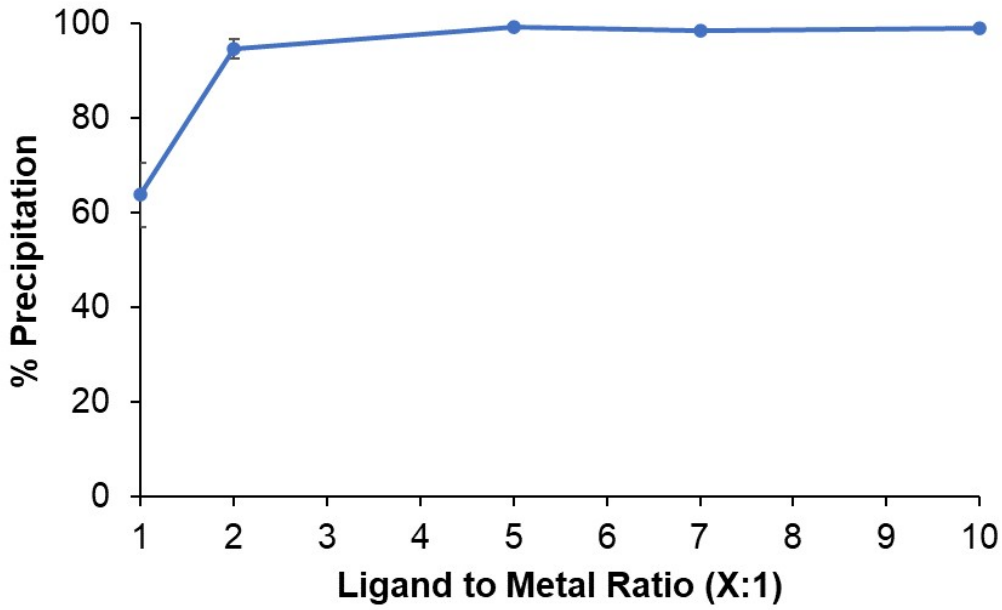

Figure S7. Varying the ligand to copper ratio with L^P – The precipitation plot of percentage precipitation vs ligand:metal ratio for L^P shows near quantitative precipitation at a lower ratio than for L^O (2:1 vs 5:1), however, a ratio of 5:1 was chosen for all further precipitation experiments as quantitative precipitation was achieved at this ratio and it also facilitated direct comparison between L^O and L^P.

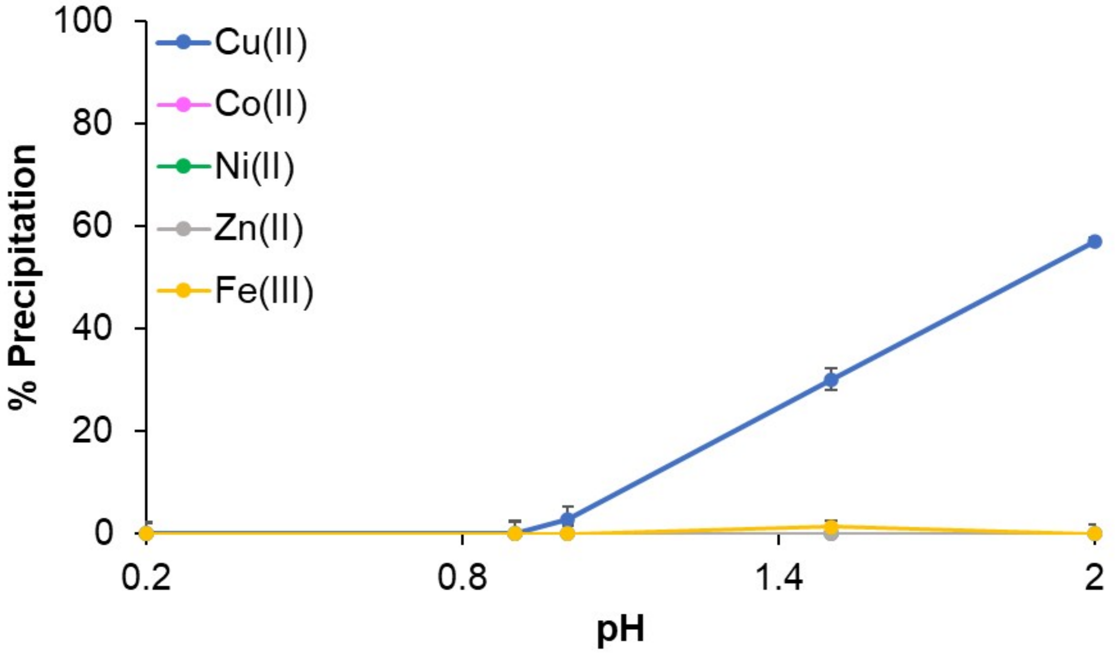

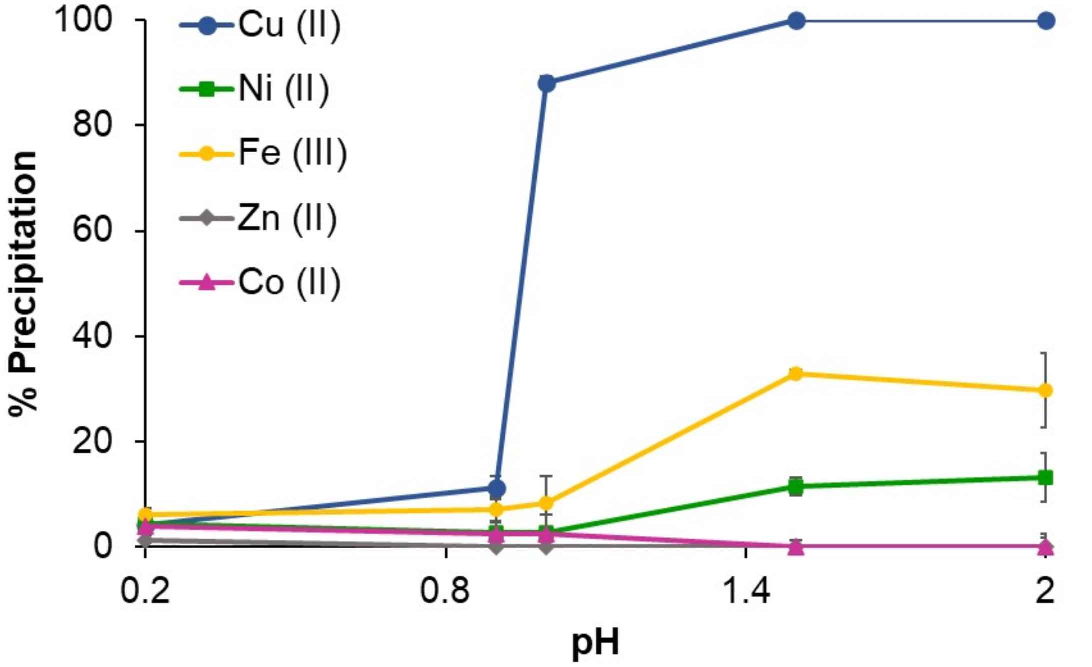

Figure S8. Precipitation plots including Fe(III) – (Top) Precipitation plot for L^O at a ligand to copper ratio of 5:1 from equimolar mixed-metal solutions containing Fe(III) over the pH range 0.2 to 2. (Bottom) Precipitation plot for L^P at a ligand to copper ratio of 5:1 from equimolar mixed-metal solutions containing Fe(III) over the same pH range as for L^O. The solid lines are drawn for ease of interpretation only.

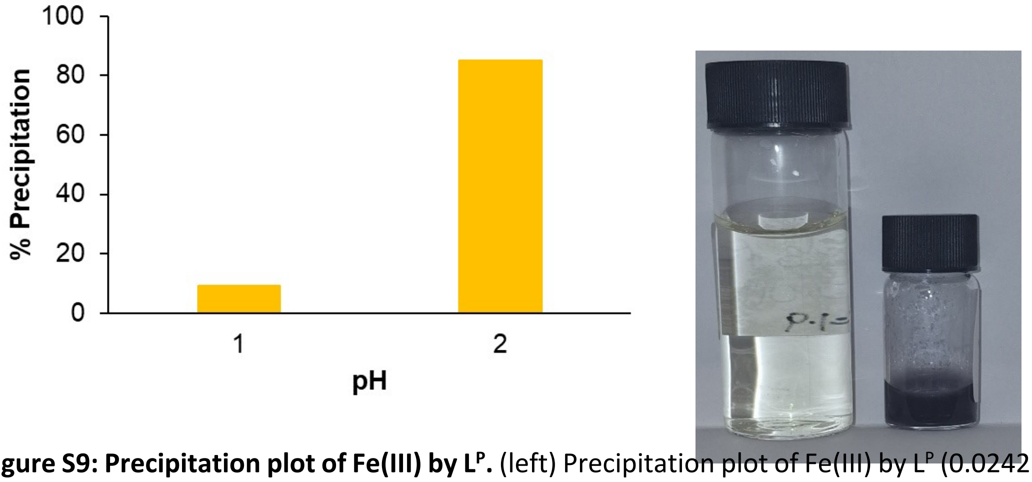

Figure S9: Precipitation plot of Fe(III) by L^P. (left) Precipitation plot of Fe(III) by L^P (0.0242 g, 0.1 mmol) at a 5:1 ligand:Fe ratio at pH=1, 2. The plot shows that high uptake of Fe(III) occurs at higher pH while minimal uptake is observed at lower pH. However, at pH=1 a change in colour of the aqueous solution is observed (right) after 1 h from pale yellow to dark purple. This suggests that an aqueous soluble Fe(III) complex forms. Given Fe(III) can form a wider variety of complexes, we hypothesise that the presence of Fe(III) in solution results in the formation of mixed metal precipitates that form more readily than single metal precipitates, resulting in precipitation of all metals at lower pH, as seen above in Figure S8.

Experimental: Solid L^P (0.0242 g, 0.1 mmol) was added to a vial with a magnetic stir bar followed by a solution of $FeCl_3$ (2 mL, 0.02 mmol either in 0.01 M H_2SO_4 (pH=2) or 0.1 M H_2SO_4 (pH=1)). Samples were stirred for 24 h at 500 rpm at room temperature (20 °C). The stir bar was then removed and the samples centrifuged for 5 minutes at 4000 rpm to separate the solids from the supernatant. The supernatants and feed samples were diluted x100 in 2% nitric acid for analysis by ICP-OES to determine metal content. All experiments were carried out in duplicate.

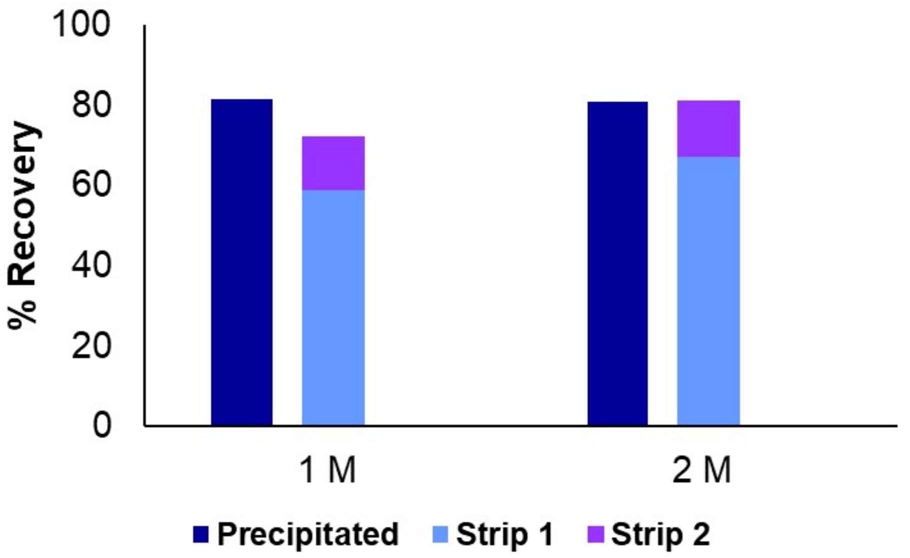

Aqueous Solution	Cu in loaded precipitate (mg L^{-1})	Cu in Strip Solution 1 (mg L^{-1})	Cu in Strip Solution 2 (mg L^{-1})	% Stripping (Strip 1)	% Stripping (strip 2, cumulative)
1 M Strip	517	375	83	72	88
2 M Strip	512	427	119	83	100

Figure S10. Determination of optimum strip conditions for L^O – (Top) Recovery plot showing the percentage copper precipitated by L^O (dark blue bars) and the subsequent percentage of copper recovered from the loaded-precipitate using 1 M H_2SO_4 or 2 M H_2SO_4 strip solutions (light blue and purple bars). After 2 contacts, quantitative copper recovery was achieved using 2 M H_2SO_4, while a third contact would be required with the 1 M H_2SO_4 strip solution to achieve complete recovery. Therefore, 2 M H_2SO_4 was chosen as the optimum strip solution. (Bottom) Table detailing the analytical data presented in the recovery plot, showing the complete recovery of copper with the 2 M H_2SO_4 solution vs the incomplete recovery with a 1 M H_2SO_4 strip solution.

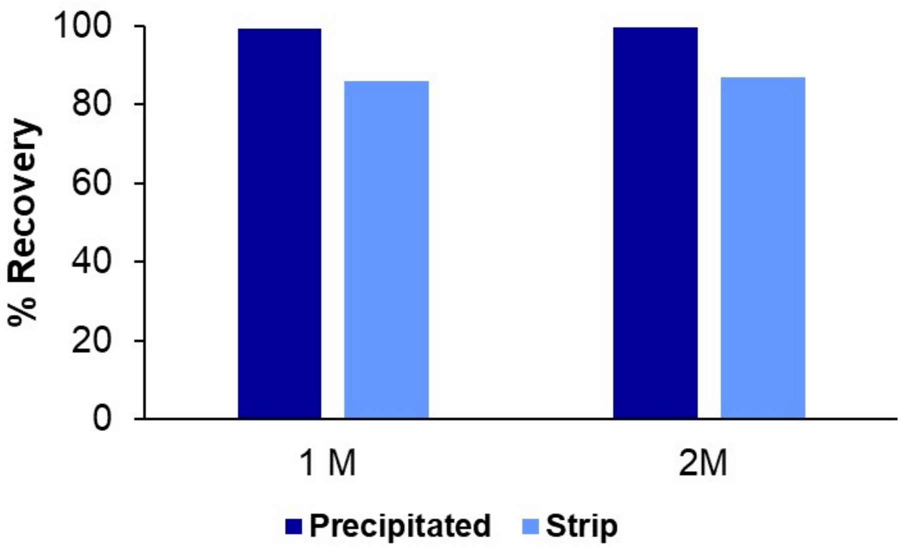

Aqueous Solution	Cu in loaded precipitate (mg L^{-1})	Cu in Strip Solution (mg L^{-1})	% Stripping (Strip 1)
1 M Strip	582	505	86
2 M Strip	583	511	88

Figure S11. Determination of optimum strip conditions for L^{P} – (Top) Recovery plot showing the percentage copper precipitated by L^{P} (dark blue bars) and the subsequent percentage of copper recovered from the loaded-precipitate using 1 M H_2SO_4 or 2 M H_2SO_4 strip solutions. After 1 contact, both strip solutions afford a high percentage recovery from the loaded precipitate, with the 2 M H_2SO_4 solution recovering slightly more. The 2 M H_2SO_4 solution was chosen as the optimum strip solution for all further experiments in order to maintain consistency with the L^{O} results. (Bottom) Table detailing the analytical data presented in the recovery plot, showing near quantitative stripping with both 1 M and 2 M H_2SO_4 solutions after one contact.

Table S2. Analytical data for L^O recycling experiments – The concentrations of each solution recorded by ICP-OES are given below for the recycling experiments carried out with L^O.

Aqueous Solution	Cu in solution cycle 1 (mg L^{-1})	Cu in solution cycle 2 (mg L^{-1})	Cu in solution cycle 3 (mg L^{-1})
Cu Stock Solution	615	615	629
Raffinate	105	61	43
Water Rinse (pre strip)	10	10	10
Strip 1	394	447	457
Strip 2	97	87	99
Strip 3	62	29	30
Water Rinse 1(post strip)	17	23	-
Water Rinse 2(post strip)	11	11	-
Water Rinse 3(post strip)	9	10	-

Table S3. Analytical data for L^P recycling experiments – The concentrations of each solution recorded by ICP-OES are given below for the recycling experiments carried out with L^P.

Aqueous Solution	Cu in solution cycle 1 (mg L^{-1})	Cu in solution cycle 2 (mg L^{-1})	Cu in solution cycle 3 (mg L^{-1})
Cu Stock Solution	576	576	576
Raffinate 1	61	115	84
Water Rinse (pre strip)	9	9	9
Strip 1	452	402	440
Strip 2	34	32	31
Strip 3	11	10	10
Water Rinse 1 (post strip)	10	9	-
Water Rinse 2 (post strip)	8	8	-
Water Rinse 3 (post strip)	8	8	-

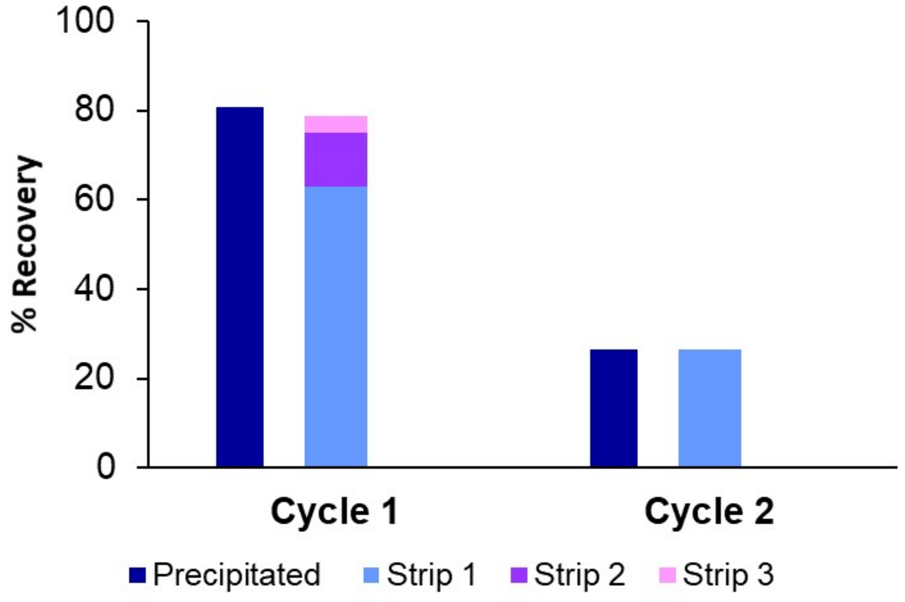

Aqueous Solution	Cu in solution cycle 1 (mg L^{-1})	Cu in solution cycle 2 (mg L^{-1})
Cu Stock Solution	583	575
Raffinate 1	116	413
Water Rinse (pre strip)	2	5
Strip 1	364	169
Strip 2	73	30
Strip 3	22	-

Figure S12. Recycling experiments with L^O without H_2O washing – (Top) Recovery plot showing the performance of L^O over two cycles without a H_2O rinse between cycles. The first cycle shows high precipitation of copper by L^O with complete stripping of the loaded precipitate achieved after three strip steps using 2 M H_2SO_4. However, a large drop in performance is observed for cycle 2, with only ca. 30% copper recovery. This is due to the entrained acid from the strip steps of cycle 1, which results in a solution that is too acidic for L^O to afford quantitative precipitation of copper. (Bottom) Table detailing the analytical data presented in the recovery plot, highlighting the drop in performance of L^O from cycle 1 to cycle 2.

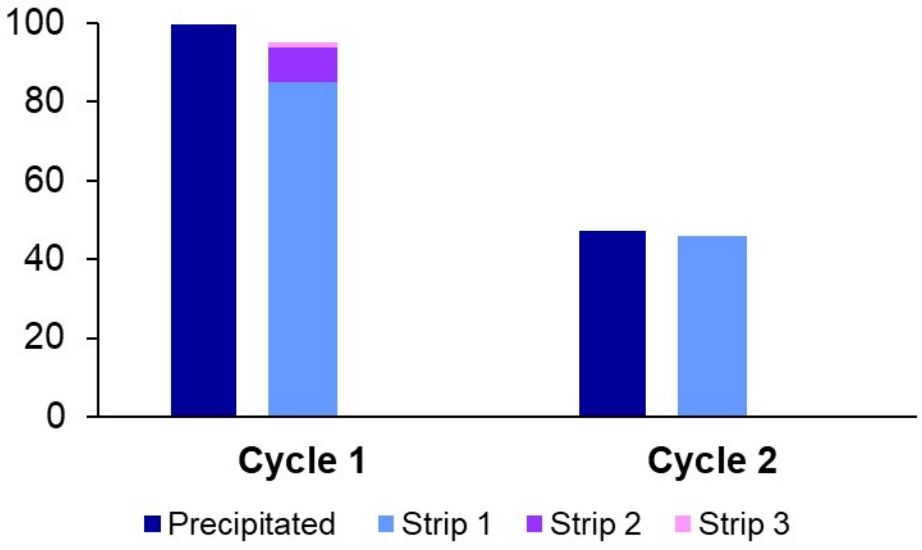

Aqueous Solution	Cu in solution cycle 1 (mg L^{-1})	Cu in solution cycle 2 (mg L^{-1})
Cu Stock Solution	583	575
Raffinate 1	1	308
Water Rinse (pre strip)	2	6
Strip 1	495	261
Strip 2	53	40
Strip 3	7	-

Figure S13. Recycling experiments with L^P without H_2O washing – (Top) Recovery plot showing the performance of L^P over two cycles without a H_2O rinse between cycles. The first cycle shows high precipitation of copper by L^P with complete stripping of the loaded precipitate achieved after three strip steps using 2 M H_2SO_4. Again, a large drop in performance is observed for cycle 2 (ca 50% recovery), as a result of the entrained acid from the strip steps of cycle 1. (Bottom) Table detailing the analytical data presented in the recovery plot, highlighting the drop in performance of L^P from cycle 1 to cycle 2.

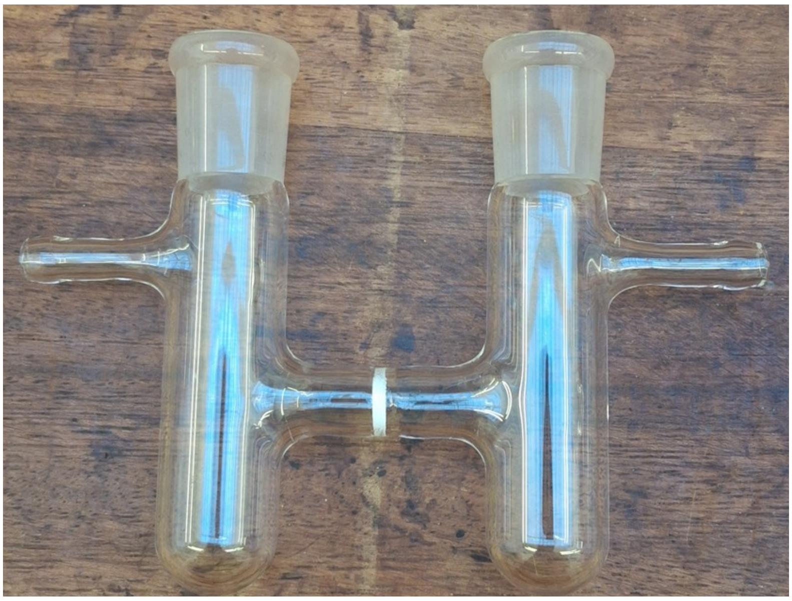

Figure S14: H-tube apparatus used to quantify ligand loss. To the H-tube shown above, L^O (0.0227 g, 0.1 mmol, 5:1 ligand:Cu) was added to one side along with a stir bar and a solution of $CuSO_4$ (0.02 mmol / H_2O). The solution was stirred for 1 h and then the raffinate was decanted by tilting the H-tube so that the raffinate would be collected in the empty side of the tube, while all of the solids would remain in the other. The H-tube was then allowed to dry before weighing. Then, the solids were washed with acetone to dissolve any free ligand that remained. The washings were filtered off as before and the H-tube dried and weighed. The difference in weight should correspond to 4 equivalents of the ligand, with 1 equivalent used to precipitate the copper. A summary of the results are given below:

Sample	Mass / g	Difference / g
H-tube/stir bar/dry complex	60.6183	
H-tube/stir bar/washed complex	60.6003	0.0180
Expected difference		0.0182

These results show that 99% of the 4 equivalents of L^O that are not involved in copper precipitation remain as a solid in the reaction vessel and are not lost to the aqueous phase.

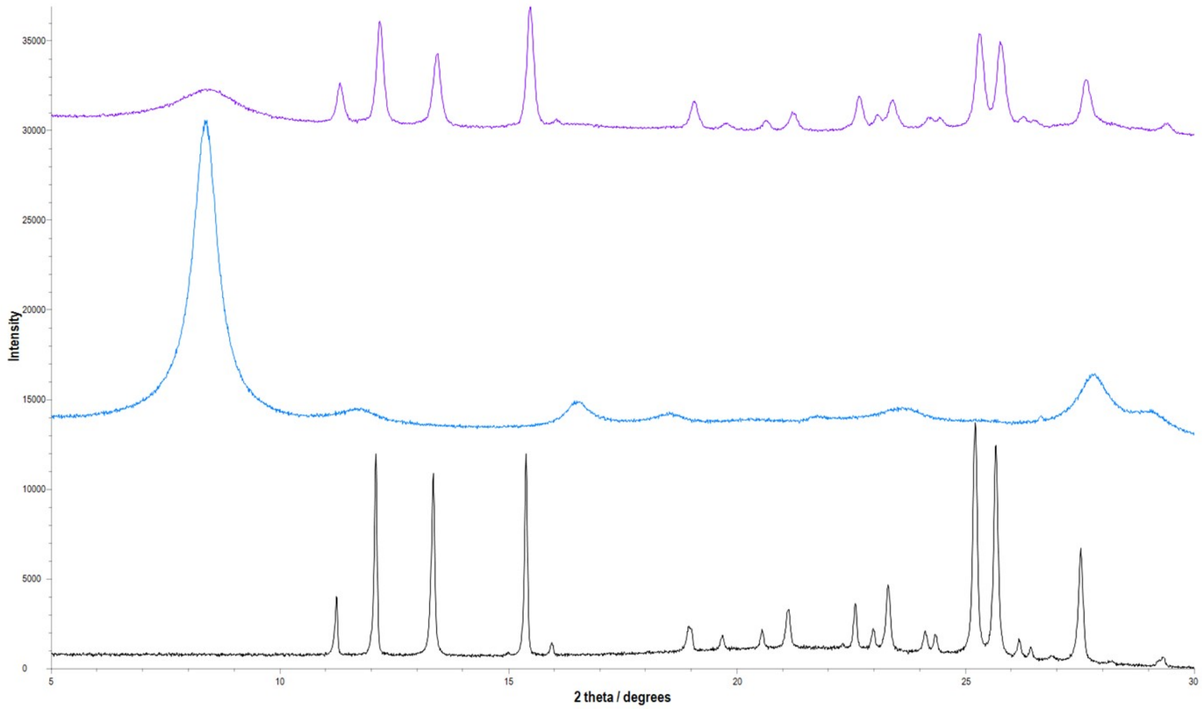

Figure S15: Stacked PXRD patterns of L^O, $[Cu(L^O)]n$ and $L^O/[Cu(L^O)]n$. Solid L^O (0.0224 g, 0.1 mmol, 5:1 ligand:Cu) was added to a vial with a solution of $CuSO_4$ (0.02 mmol in H_2O) and stirred for 1 h. The solution was then filtered and washed with water to remove any entrained copper and the powder was allowed to air dry. The PXRD pattern of this solid (purple trace) was then compared to the patterns of free L^O (black trace) and the $[Cu(L^O)]n$ complex (blue trace). The PXRD pattern of the filtered sample shows peaks corresponding to both free L^O and the $[Cu(L^O)]n$ complex, which consolidates the results from the H-tube experiment that suggest the excess ligand not involved in complexation with the copper remains as a solid and is not lost to the aqueous phase.

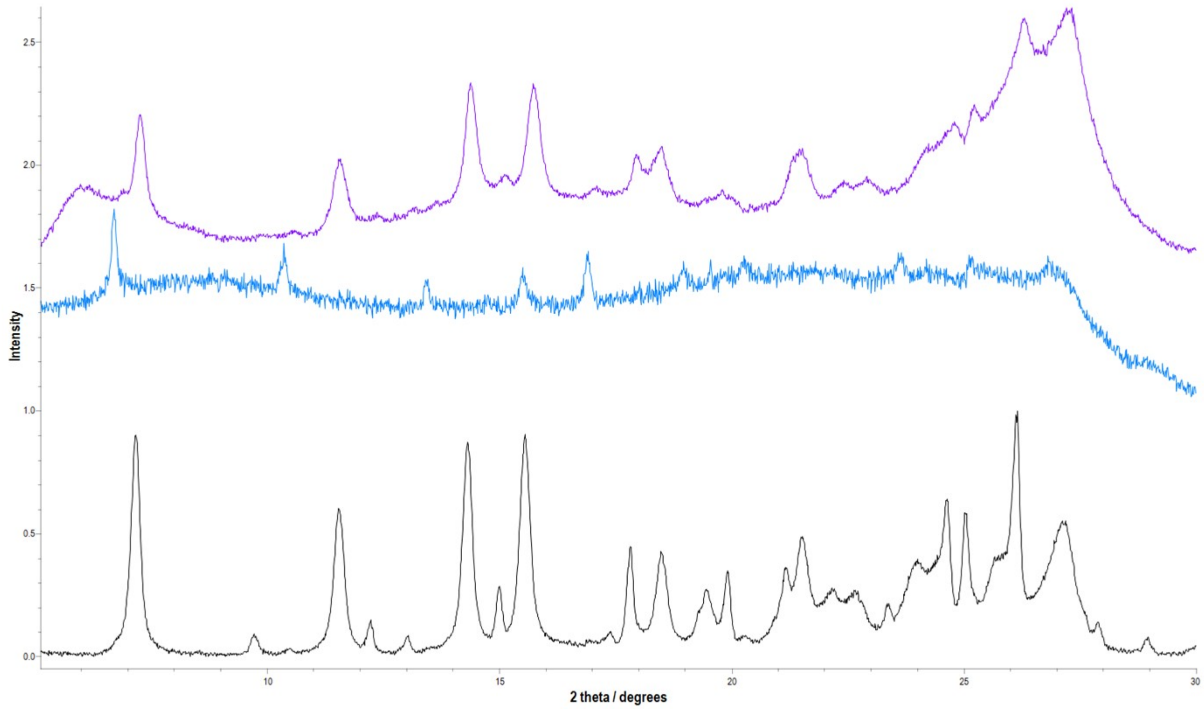

Figure S16: Stacked PXRD patterns of L^P, $[Cu(L^P)]n$ and $L^P/[Cu(L^P)]n$. Solid L^P (0.0242 g, 0.1 mmol, 5:1 ligand:Cu) was added to a vial with a solution of $CuSO_4$ (0.02 mmol in H_2O) and stirred for 1 h. The solution was then filtered and washed with water to remove any entrained copper and the powder was allowed to air dry. The PXRD pattern of this solid (purple trace) was then compared to the patterns of free L^P (black trace) and the $[Cu(L^P)]n$ complex (blue trace). The majority of the peaks observed in the powder pattern of the filtered sample correspond to free L^P with broad amorphous peaks at 6° and 28° 2theta confirming the presence of the $[Cu(L^P)]n$ complex, which confirms that the excess ligand not involved in complex formation remains as a solid and is not lost to the aqueous phase.

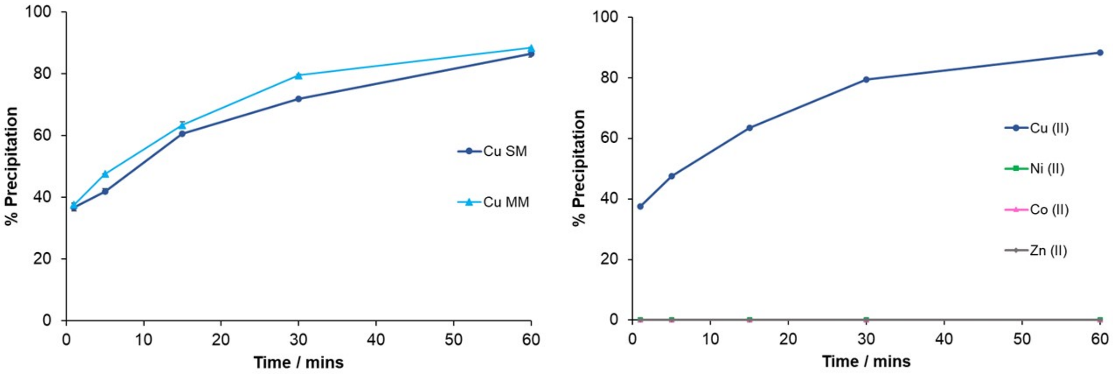

Figure S17: Kinetic plots for the precipitation of $[Cu(L^O)]_n$ at pH 5. (a) Precipitation plot (%) of $[Cu(L^O)]_n$ from a single metal copper solution (light blue) or mixed-metal solution (dark blue) over a specified time period. (b) Precipitation plot (%) of $[Cu(L^O)]_n$ from the mixed-metal solution (dark blue) given in (a) showing no precipitation of any other metal. The kinetic plots show that a 1 h timeframe is necessary to achieve maximum uptake of copper, with a maximum 12% percentage increase when the ionic strength of the solution is increased (single metal vs mixed-metal).

Experimental: Solid L^O (0.0224 g, 0.1 mmol) was added to a vial with a stir bar and either a solution of $CuSO_4$ (0.02 mmol, 2 mL) or a mixed-metal solution ($CuSO_4$ / $NiSO_4$ / $CoSO_4$ / $ZnSO_4$, 0.02 mmol each, 2mL) and placed in a Fisherbrand mini shaker. After the specified time had passed (1, 5, 15, 30, 60 mins), samples were removed and centrifuged for 5 minutes at 4000 rpm to separate the solids from the supernatant. The supernatants and feed samples were diluted x100 in 2% nitric acid for analysis by ICP-OES to determine metal content. All experiments were carried out in duplicate.

T=0 T=1 min T=5 mins T=10 mins T=30 mins T=60 mins

Figure S18: Time series to determine the settling time of $[\mathrm{Cu}(\mathrm{L^{O}})]_n$ under ambient conditions. The images indicate a settling time of 30 minutes for $[\mathrm{Cu}(\mathrm{L^{O}})]_n$, with the majority of the material separated from the supernatant after 5 minutes.

Pyrazole

T=0 T=1 min T=5 mins T=10 mins T=30 mins T=60 mins

Figure S19: Time series to determine the settling time of $[\mathrm{Cu}(\mathrm{L^{P}})]_n$ under ambient conditions. The images indicate a settling time of approximately 5 minutes for $[\mathrm{Cu}(\mathrm{L^{P}})]_n$, however, given the material has a tendency to stick to the inside of the reaction vessel, an accurate settling time cannot be reported.

Section 4: Analytical ICP data

Table S4. Analytical data for waste PCB leachate– The concentrations of all metals present in concentrations greater than 0.01 mg L^{-1} recorded by ICP-MS for the e-waste leachate are given below.

Element	Concentration in ICP sample (mg L^{-1})	Concentration in neat leach solution (mg L^{-1})
Al	0.00400	4.00
Ti	0.00005	0.05
Cr	0.00013	0.13
Mn	0.00099	0.99
Fe	0.11391	113.91
Co	0.00042	0.42
Ni	0.07573	75.73
Cu	0.37205	372.05
Zn	0.00756	7.56
As	0.00008	0.08
Mo	0.00006	0.06
Cd	0.00001	0.01
Sn	0.02562	25.62
Sb	0.00038	0.38
Pb	0.04306	41.74

Table S5. Summary of ICP-OES wavelengths– The wavelengths used for all metals analysed by ICP-OES are summarised in the table below.

Element	Wavelength / nm
Cu	327.393
Ni	221.648
Co	228.616
Zn	213.857
Al	396.153
Cr	205.560
Mn	257.610
Fe	238.204
Sn	283.998
Pb	220.353
Y (internal standard)	324.227

Table S6. Summary of ICP-MS isotopes – The isotopes used for all metals analysed by ICP-MS are summarised in the table below.

Element	Isotope
Al	27
Ti	47
Cr	52
Mn	55
Fe	56
Co	59
Ni	60
Cu	63
Zn	66
As	75
Mo	95
Cd	111
Sn	118
Sb	121
Pb	207

Section 5: Pawley refinement of L^O PXRD Data

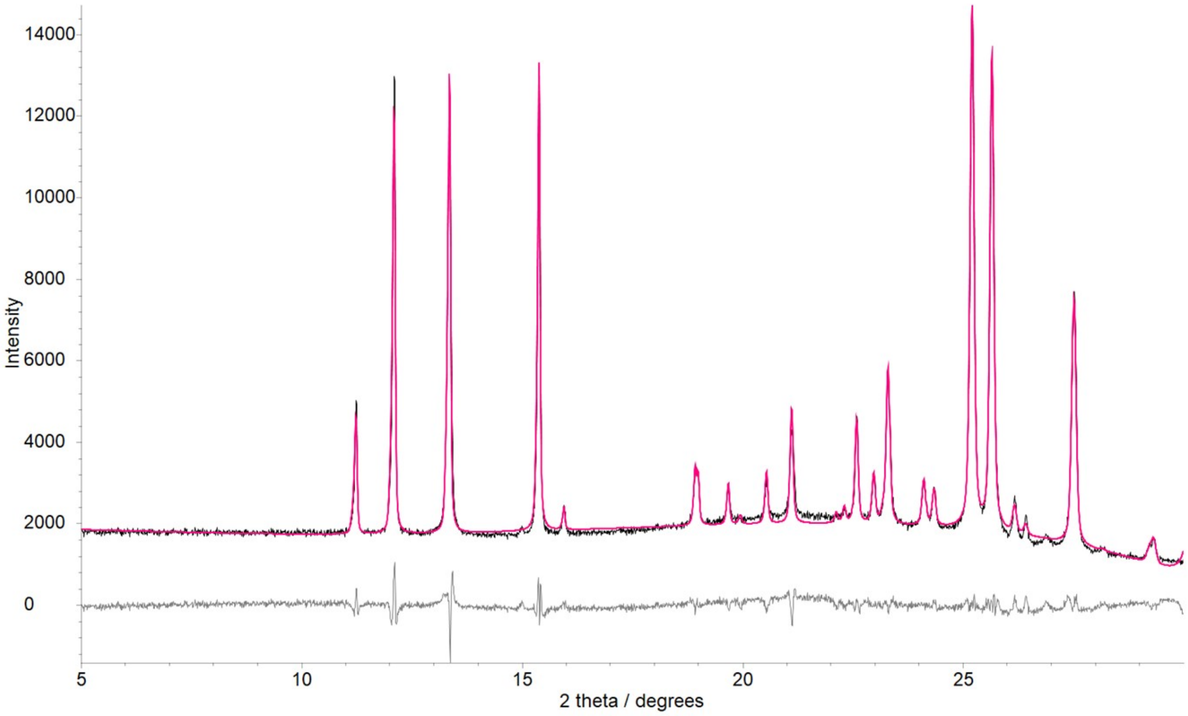

Unit Cell Parameter	Single Crystal	Pawley Fit	% Difference
a	7.4675(3)	7.6367(2)	2.24
b	9.3690(4)	9.3359(5)	0.35
c	14.5222(6)	14.6351(8)	0.77
β	92.911(2)	92.922(4)	0.01

Figure S20. PXRD Pawley Refinement of L^O – The observed pattern of the bulk L^O ligand is shown in black with the fit calculated using a Pawley refinement shown in pink. The difference profile is shown in grey. A good match between the refined unit cell parameters from analysis of the PXRD data and the unit cell parameters from the single crystal x-ray diffraction data refinement (shown above) confirms that the two phases are the same.

Section 6: Summary of XRF data

Table S7. Summary of XRF data recorded for $[Cu(L^O)]_n$ – The composition of $[Cu(L^O)]_n$ as determined by XRF is presented in the table below, with over 90% of the sample characterised as copper. The only other metal detected was aluminium, which likely originated from the vial cap. It should be noted that the XRF set-up used in this work did not have the capability to detect C, N or O, and therefore the data was used to confirm the presence of copper in the precipitate.

Element	% make-up of sample
Al	7.428
Cu	92.572
All other elements*	0

*Si, P, S, Cl, K, Ca, Sc, Ti, V, Cr, Mn, Fe, Co, Ni, Zn, Ga, Ge, As, Se, Br, Rb, Sr, Y, Zr, Nb, Mo, Ru, Rh, Ag, Cd, In, Sn, Sb, Te, I, Cs, Ba, La, Hf, Ta, W, Re, Os, Ir, Pt, Au, Hg, Tl, Pb, Bi, Mg.

Table S8. Summary of XRF data recorded for $[Cu(L^P)]_n$ – The composition of $[Cu(L^P)]_n$ as determined by XRF is presented in the table below, with over 75% of the sample characterised as copper. The only other elements detected were aluminium (vial cap contamination), phosphorus, calcium and zinc, which, given the very small percentage of the composition they comprise, likely arise from contamination from lab utensils or the vial cap. Finally, 15% of the sample was characterised as sulphur, which indicates the precipitated structure may contain some sulfate anions. As for $[Cu(L^O)]_{n}$, the high copper percentage confirms the presence of copper in the precipitate.

Element	% make-up of sample
Al	7.294
P	0.286
S	15.393
Ca	0.156
Cu	76.6
Zn	0.271
All other elements*	0

*Si, Cl, K, Sc, Ti, V, Cr, Mn, Fe, Co, Ni, Ga, Ge, As, Se, Br, Rb, Sr, Y, Zr, Nb, Mo, Ru, Rh, Ag, Cd, In, Sn, Sb, Te, I, Cs, Ba, La, Hf, Ta, W, Re, Os, Ir, Pt, Au, Hg, Tl, Pb, Bi, Mg.

Section 7: Extended MALDI mass spectrometry data

A selection of mass spectra recorded for L^O, L^P, $[Cu(L^O)]_n$ and $[Cu(L^P)]_n$ in different matrices are given below. LDI was initially tested for the ligands however no ionisation was observed, therefore tests with different matrices were undertaken.

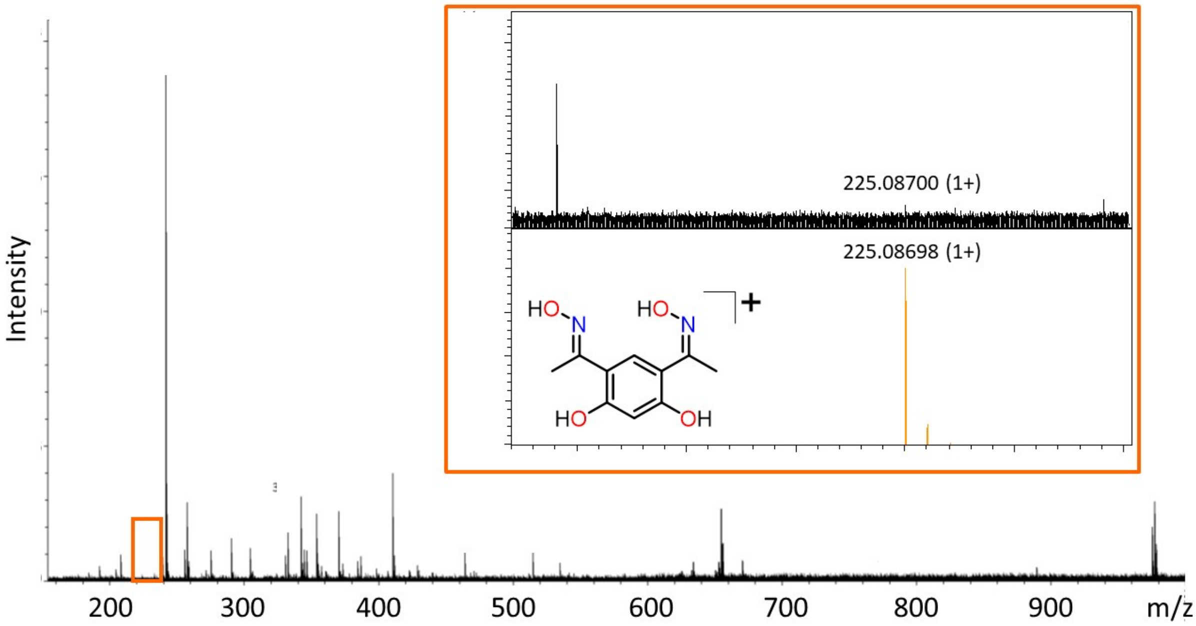

Figure S21. Full MALDI mass spectrum recorded for L^O using 2,5-dihydroxybenzoic acid (pKa=3) matrix. Magnification of the region where the monoisotopic ligand peak should appear (orange box) shows a very small peak (225.08700 m/z) that matches the calculated peak (mass error = 0.09 ppm). This shows that the ligand degrades in the acidic matrix solution, resulting in a complex spectrum of degradation products. The highest peak in the spectrum corresponds to TBA (tetrabutylammonium), a common buffer used in mass spectrometry.

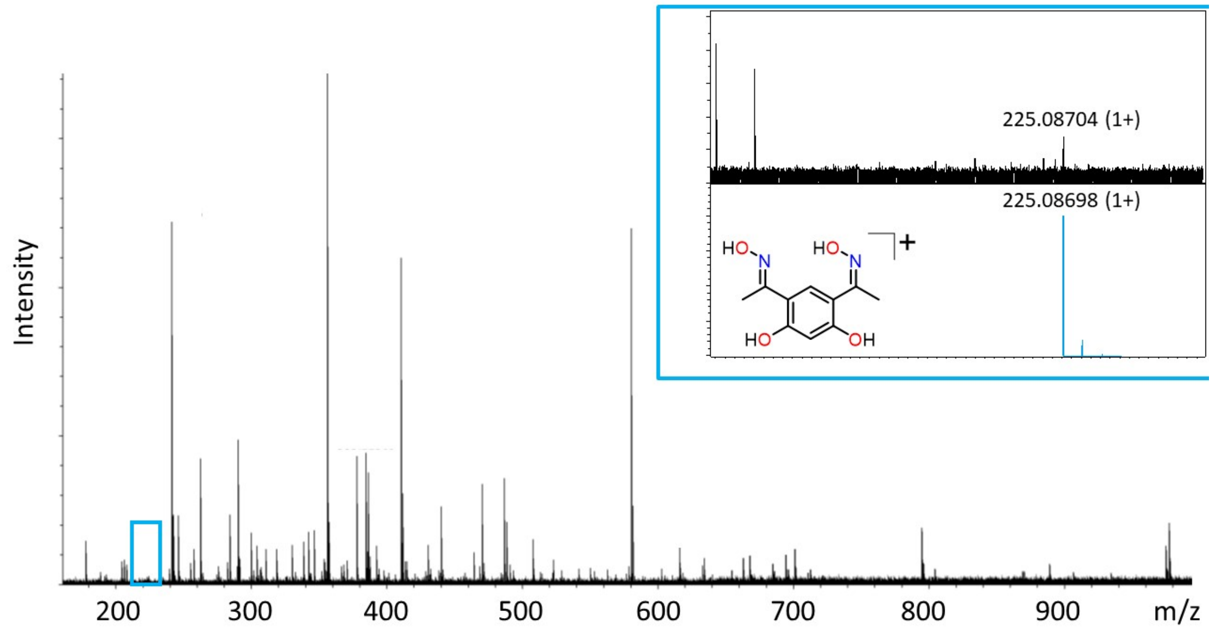

Figure S22. Full MALDI mass spectrum recorded for L^{O} using sinapinic acid (pKa=3.41) matrix. Magnification of the region where the monoisotopic ligand peak should appear (blue box) shows a small peak (225.08704 m/z) that matches the calculated peak (mass error = 0.27 ppm). The peak is slightly larger in this spectrum compared to that recorded in 2,5-dihydroxybenzoic acid. This supports the hypothesis that the acidic matrix degrades the ligand, with more degradation observed in the more acidic 2,5-dihydroxybenzoic acid matrix than in the sinapinic acid matrix.

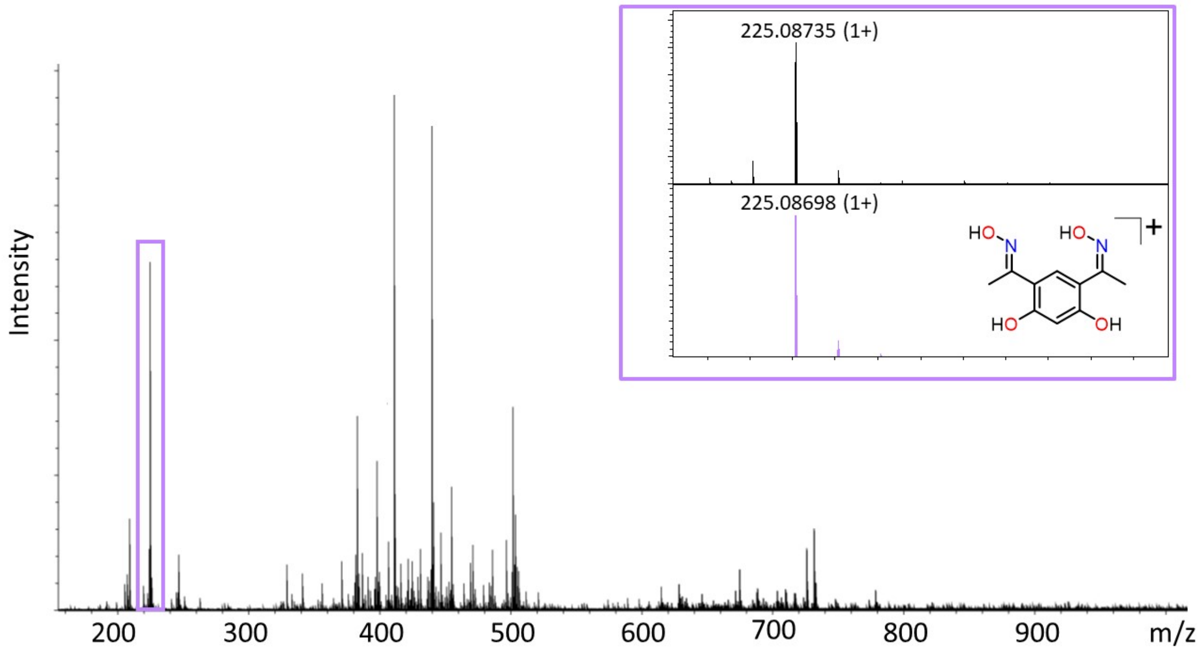

Figure S23. Full MALDI mass spectrum recorded for L^O using 4-cyano-2-nitrophenol matrix (non-acidic). Magnification of the region where the monoisotopic ligand peak should appear (purple box) shows a much larger peak (225.08735 m/z) that matches the calculated peak (mass error = 1.64 ppm). This further consolidates the hypothesis that the ligand degrades in acidic matrices.

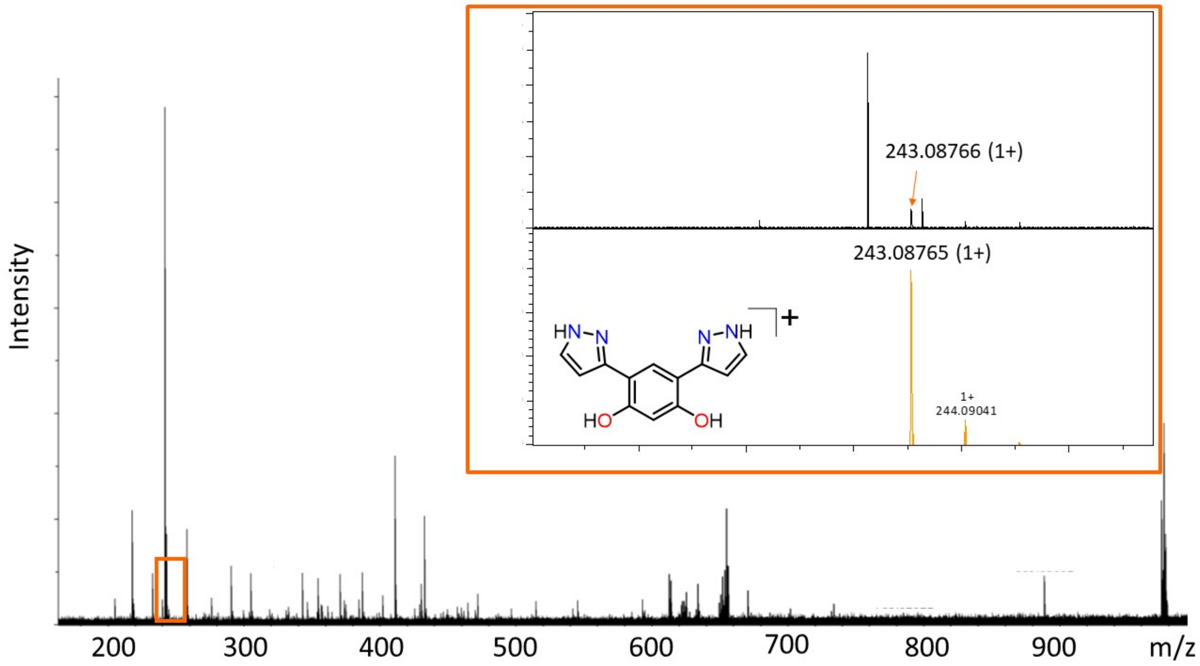

Figure S24. Full MALDI mass spectrum recorded for L^P using 2,5-dihydroxybenzoic acid (pKa=3) matrix. Magnification of the region where the monoisotopic ligand peak should appear (orange box) shows a small peak (243.08766 m/z) that matches the calculated peak (mass error = 0.04 ppm). Less degradation is observed for L^P compared to L^O, with a slightly larger ligand peak observed. This is likely because L^O can be hydrolysed in acid however L^P is resistant to hydrolysis, making L^P slightly more resilient to degradation by the acidic matrices.

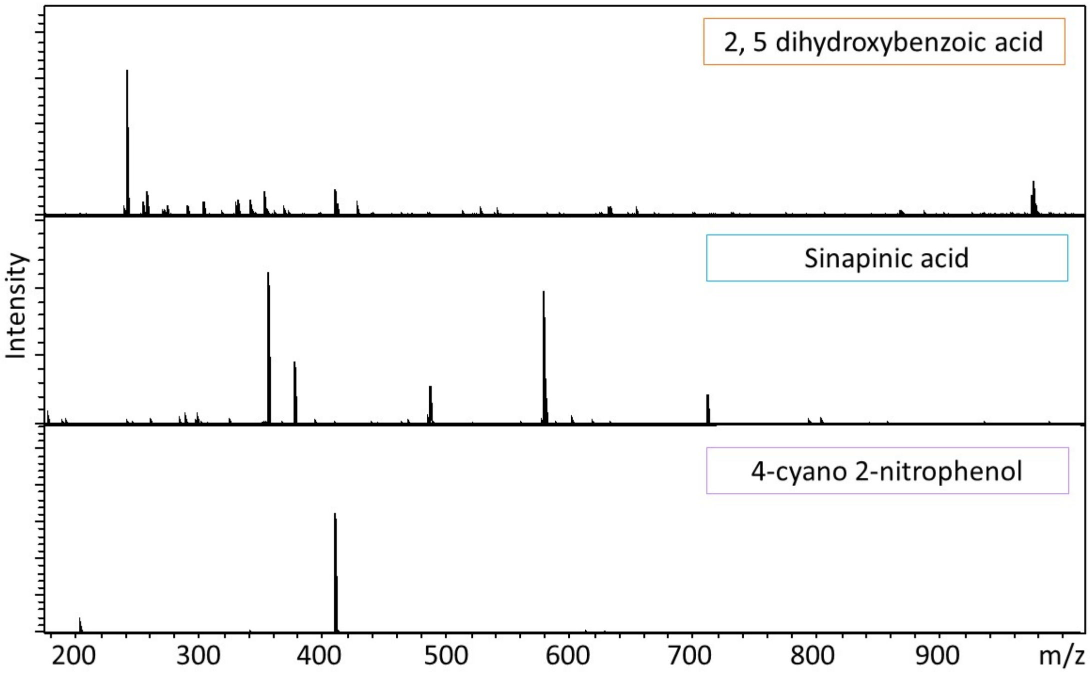

Figure S25. Stacked MALDI mass spectra recorded for $[Cu(L^O)]_n$ in different matrices. The full MALDI mass spectra for $[Cu(L^O)]_n$ in 2,5-dihydroxybenzoic acid (top), sinapinic acid (middle) and 4-cyano-2-nitrophenol (bottom) matrices are shown above. The spectra in the acidic matrices (top and middle) are complex with no discernible peaks corresponding to L^O or $[Cu(L^O)]_n$. As discussed previously, the acidic matrices cause the ligand to degrade and consequently the complexes, which are stripped in acid, therefore making this choice of matrix unsuitable. Only two peaks are observed in the 4-cyano-2-nitrophenol spectrum, which do not correspond to any L^O or $[Cu(L^O)]_n$ species and likely arise from contaminants, given the large peak 411 m/z is also present in the 2,5-dihydroxybenzoic acid spectrum. This suggests that while the complex does not degrade in the 4-cyano-2-nitrophenol matrix, it also does not ionise, resulting in no peaks in the spectrum.

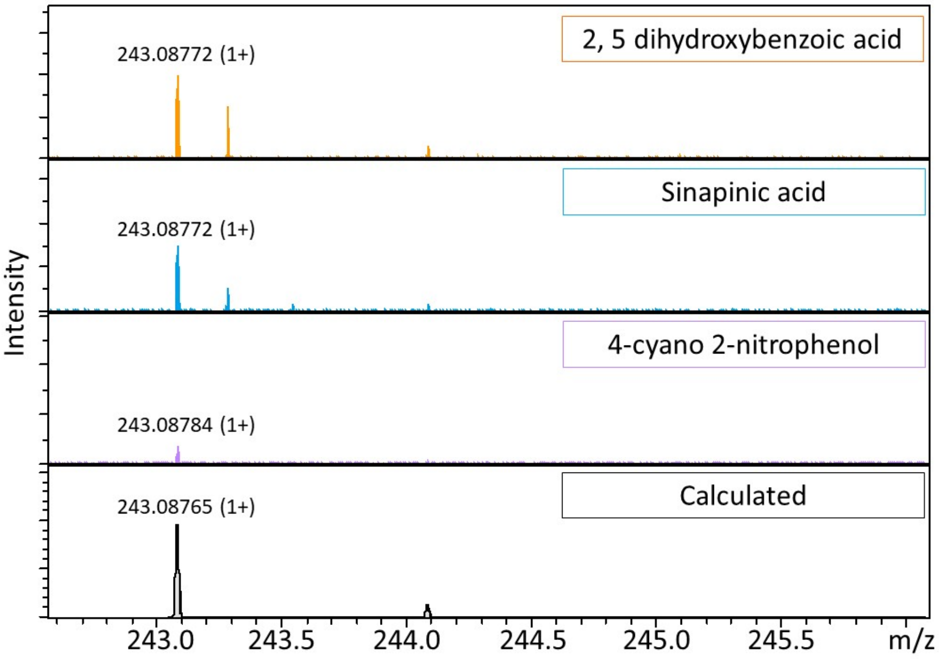

Figure S26. Stacked MALDI mass spectra recorded for $[Cu(L^P)]_n$ in different matrices. Partial MALDI mass spectra for $[Cu(L^P)]_n$ in 2,5-dihydroxybenzoic acid (orange), sinapinic acid (blue) and 4-cyano-2-nitrophenol (purple) matrices are shown above, focusing on the monoisotopic ligand peak. The spectra in the acidic matrices (orange and blue) show a larger ligand peak compared to a very small ligand peak in the 4-cyano-2-nitrophenol spectrum, which confirms more complex degradation in the acidic matrices and minimal complex degradation in the non-acidic matrix.

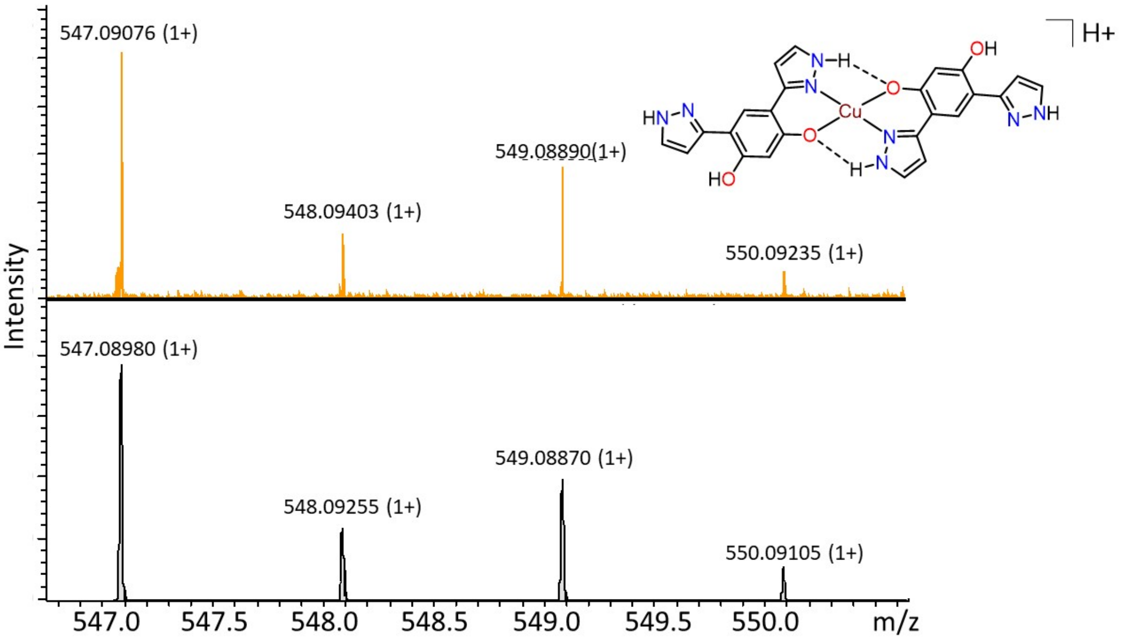

Figure S27. Partial MALDI mass spectrum recorded for $[Cu(L^P)]_n$ in 2,5-dihydroxybenzoic acid. Partial MALDI mass spectrum for $[Cu(L^p)]_n$ in 2,5-dihydroxybenzoic acid (orange, calculated in black) showing the monoisotopic complex peak for $[Cu(L^P)_2]^+$ (mass error = 1.75 ppm). Despite the high degradation of the complex in this matrix, good ionisation was achieved, which resulted in some species corresponding to $[Cu(L^p)]_n$ appearing in the mass spectrum.

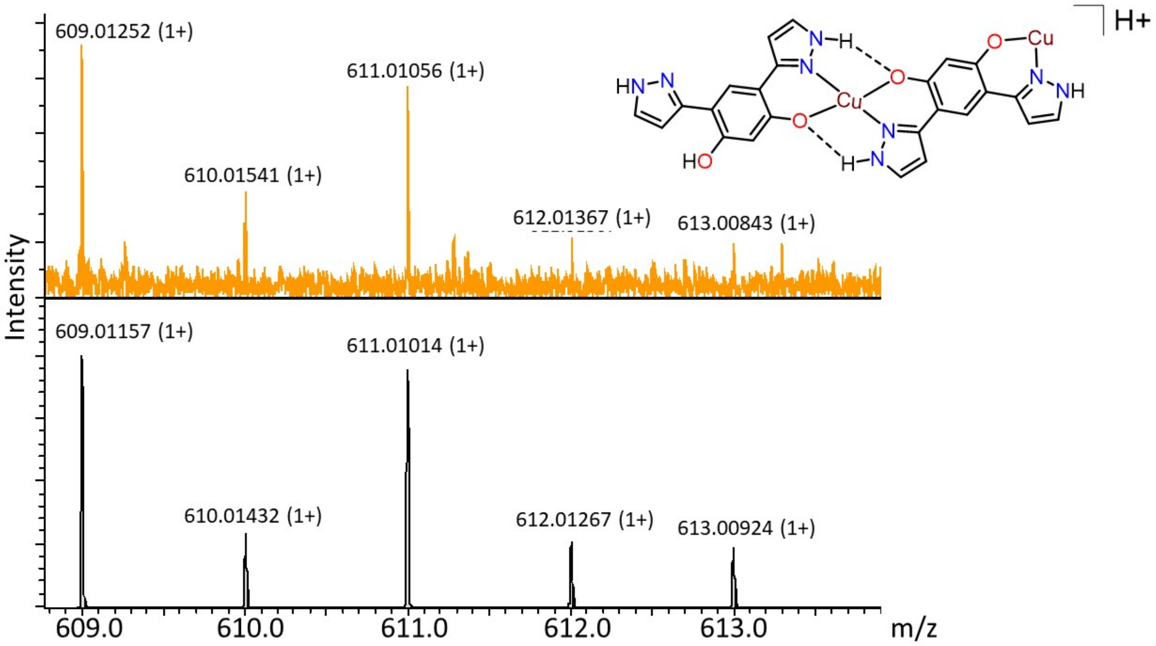

Figure S28. Partial MALDI mass spectrum recorded for $[Cu(L^P)]_n$ in 2,5-dihydroxybenzoic acid. Partial MALDI mass spectrum for $[Cu(L^p)]_n$ in 2,5-dihydroxybenzoic acid (orange, calculated in black) showing the monoisotopic complex peak for $[Cu_2(L^P)_2]^+$ (mass error = 1.56 ppm). Although the $[Cu_2(L^P)_2]^+$ fragment is observed in this spectrum, there are some other peaks present likely due to other degradation species that complicate the spectrum. However, this still provides good evidence that extended ligand – metal complexes are forming upon precipitation.

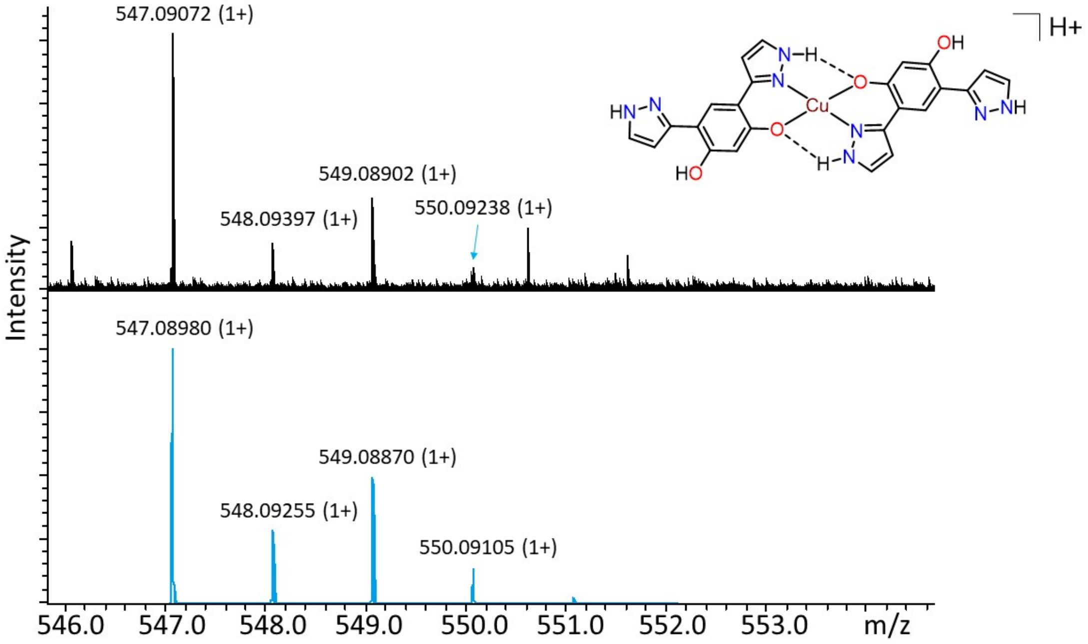

Figure S29. Partial MALDI mass spectrum recorded for $[Cu(L^P)]_n$ in sinapinic acid. Partial MALDI mass spectrum for $[Cu(L^P)]_n$ in sinapinic acid (black, calculated in blue) showing the monoisotopic complex peak for $[Cu(L^P)_2]^+$ (mass error = 1.68 ppm). A stronger isotopic pattern is observed for this fragment in sinapinic acid (pKa=3.41) compared to 2,5-dihydroxybenzoic acid (pKa=3), further consolidating that acid results in degradation of the complex.

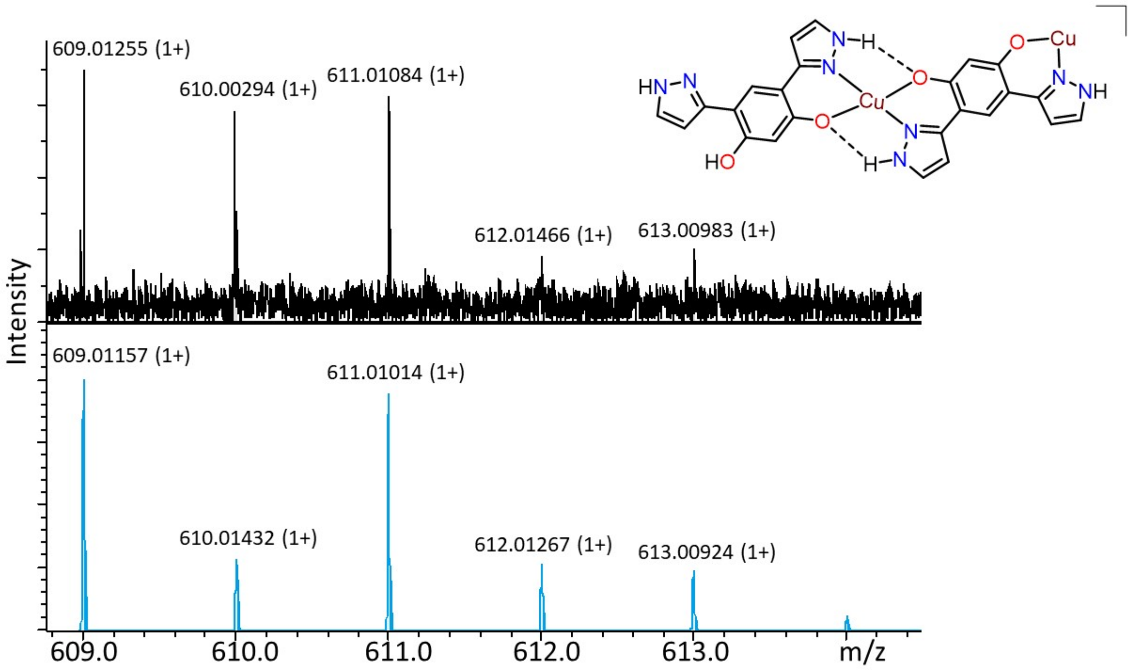

Figure S30. Partial MALDI mass spectrum recorded for $[Cu(L^P)]_n$ in sinapinic acid. Partial MALDI mass spectrum for $[Cu(L^P)]_n$ in sinapinic acid (black, calculated in blue) showing the monoisotopic complex peak for $[Cu_2(L^P)_2]^+$ (mass error = 1.68 ppm). Again, stronger isotopic pattern is observed for this fragment in sinapinic acid (pKa=3.41) compared to 2,5-dihydroxybenzoic acid (pKa=3),with no other peaks corresponding to degradation products observed.

Section 8: Summary of Life Cycle Inventory

Table S9. Life Cycle Inventory – The details of all materials and process inputs included in the life cycle inventory for both the precipitation and solvent extraction processes are given below.

Process	Materials / Assemblies	Items	Source	Quantity (per functional unit)	Unit
Precipitation	Reagents	Ligand	[1]	19.83	g
		H_2SO_4	[1]	4917.70	mL
		H_2O	[2]	3278.46	mL
	Waste	Raffinate	[3]	1639.23	mL
	Electricity	Stir plate	[2]	426.20	kW h
		Centrifuge	[2]	225.39	kW h
	Lab Equipment	Pipette (glass)	[2]	6884.78	g
		Vial (glass)	[2]	4917.70	g
	Source Material	E-waste	[4]	75.54	g
Solvent Extraction	Reagents	Ligand	[1]	575.73	mL
		Solvent (Kerosene)	[1]	1919.10	mL
		H_2SO_4	[1]	1919.10	mL
	Waste	Raffinate	[3]	1919.10	mL
	Electricity	Stir plate	[2]	38.38	kW h
	Lab Equipment	Pipette (glass)	[2]	8060.23	g
		Vial (glass)	[2]	6333.03	g
	Source Material	E-waste	[4]	64.52	g

Section 9: Crystallographic Table

L^{O}

CCDC Deposition No.	2404167
Chemical formula	$C_{10}H_{12}N_2O_4$
M_r	224.22
Crystal system, space group	Monoclinic, $P2_1/n$
Temperature (K)	100
a, *b*, *c* (Å)	7.4675 (3), 9.3690 (4), 14.5222 (6)
β (°)	92.911 (2)
V ($Å^3$)	1014.71 (7)
Z	4
Radiation type	Mo *K*α
μ (mm^{-1})	0.12
Crystal size (mm)	0.21 × 0.10 × 0.01
Data collection	
Diffractometer	Bruker *APEX*-II CCD
Absorption correction	Multi-scan *SADABS2016*/2 (Bruker,2016/2) was used for absorption correction. wR2(int) was 0.1106 before and 0.0671 after correction. The Ratio of minimum to maximum transmission is 0.9081. The λ/2 correction factor is Not present.
T_{min}, T_{max}	0.677, 0.745
No. of measured, independent and observed [$I > 2σ(I)$] reflections	43046, 1858, 1424
R_{int}	0.074
$(\sin θ/λ)_{max}$ ($Å^{-1}$)	0.604
Refinement	
$R[F^2 > 2σ(F^2)]$, $wR(F^2)$, S	0.052, 0.156, 1.07
No. of reflections	1858
No. of parameters	152
H-atom treatment	H-atom parameters constrained
$Δρ_{max}$, $Δρ_{min}$ (e $Å^{-3}$)	0.32, −0.28

References

[1] *Winnipeg sewage treatment program, SEWPCC Process Selection Report* 2011.

[2] UK Government greenhouse gas reporting: conversion factors 2024, https://www.gov.uk/government/publications/greenhouse-gas-reporting-conversion-factors-2024, 2024).

[3] S. Çapa, A. Özdemir, Z. Günkaya, A. Özkan and M. Banar, *Journal of Water Process Engineering*, 2022, **49**.

[4] J. Hong, W. Shi, Y. Wang, W. Chen and X. Li, *Waste Manag*, 2015, **38**, 357-365.